Ab initio approaches for N 2 + and N 2 + / He ions towards modeling of the N 2 + ion in cold helium plasma

Martin Beseda, S. Paláček, Florent X. Gadéa, Thierry Leininger, René Kalus, Malika Benhenni, Mohammed Yousfi

Graphical Abstract

***Ab initio* approaches for N_2^+ and N_2^+/He ions towards modeling of the N_2^+ ion in cold helium plasma.**

M. Beseda, S. Paláček, F. X. Gadéa, T. Leininger, R. Kalus, M. Benhenni, M. Yousfi

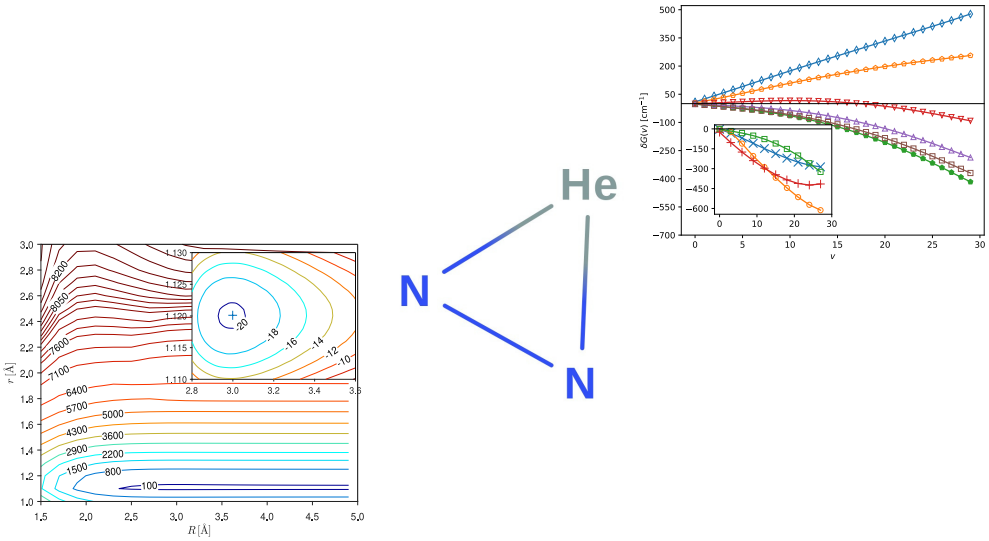

Highlights

***Ab initio* approaches for N_2^+ and N_2^+/He ions towards modeling of the N_2^+ ion in cold helium plasma.**

M. Beseda, S. Paláček, F. X. Gadéa, T. Leininger, R. Kalus, M. Benhenni, M. Yousfi

- $[N_2/He]^+$ interaction comes into play when cold rare-gas plasmas leave the interior of their generators and get into contact with environment species.
- Cold-plasmas exhibit useful properties in medicinal applications, surface treatment, food storage, and/or spacecraft propulsion.
- The main goal of the present study is to perform a comprehensive series of test electronic-structure calculations using various *ab initio* approaches in order to (mainly) assess the reliability of employed methods and their practicability in dynamical calculations.

Ab initio approaches for N_2^+ and N_2^+/He ions towards modeling of the N_2^+ ion in cold helium plasma.

M. Beseda[a], S. Paláček[a,b], F. X. Gadéa[c], T. Leininger[c], R. Kalus[a,b], M. Benhenni[d], M. Yousfi[d]

[a] *IT4Innovations National Supercomputing Center, VŠB–Technical University of Ostrava, 17. listopadu 2172/15, Ostrava–Poruba, 70800, Czech Republic*
[b] *Department of Applied Mathematics, Faculty of Electrical Engineering and Computer Science, VŠB–Technical University of Ostrava, 17. listopadu 2172/15, Ostrava–Poruba, 70800, Czech Republic*
[c] *Laboratoire de Chimie et de Physique Quantiques, IRSAMC & UMR5626 du CNRS, Université Toulouse III – Paul Sabatier, Cedex 09, Toulouse, 31062, France*
[d] *Laboratoire Plasma et Conversion d'Energie, LAPLACE & UMR5213 du CNRS, Université de Toulouse III Paul Sabatier, 118 route de Narbonne, Toulouse, 31062, France*

Abstract

As a first step towards realistic modeling of transport properties of the N_2^+ ion in helium gas, detailed investigations of the electronic structure of the ion as well as the N_2^+/He collision complex have been performed with the main focus on computational efficiency and accuracy. A broad range of correlation consistent basis sets and representative orbital spaces have been considered for both computationally cheap multi-configuration self-consistent field (MCSCF) methods and benchmark multi-reference configuration interaction (MRCI) approaches. It has been found that the computationally advantageous MCSCF approach, even if combined with basis sets of moderate sizes, leads to an acceptable accuracy and is thus suitable for direct dynamics simulations of N_2^+/He collisions to be addressed in subsequent works.

Keywords: cold plasma, dinitrogen cation, nitrogen, helium, MCSCF,

Email addresses: martin.beseda@vsb.cz (M. Beseda), stanislav.palacek@vsb.cz (S. Paláček), gadea@irsamc.ups-tlse.fr (F. X. Gadéa), thierry.leininger@irsamc.ups-tlse.fr (T. Leininger), rene.kalus@vsb.cz (R. Kalus), malika.benhenni@laplace.univ-tlse.fr (M. Benhenni), yousfi@laplace.univ-tlse.fr (M. Yousfi)

1. Introduction

The main focus of these studies is to perform numerical modelings and provide a thorough understanding of the processes responsible for interactions of active species formed in cold, non-thermal helium plasmas (as a representative of a more general class of cold rare-gas plasmas) with the environment (air and its most abundant component, nitrogen, in particular). This interaction comes into play when cold rare-gas plasmas leave the interior of their generators and get into contact with environment species. As a result, secondary, tertiary, and other generations of active species are formed which have been shown several times to lie behind possible practical applications of the cold rare-gas plasmas. In particular, medical applications are frequently mentioned in the literature [1, 2, 3] including blood coagulation, surface sterilization, wound healing, and cancer treatment (for a comprehensive review see, e.g., [3]), but, more widely, cold rare-gas plasmas are also used in the activation of plants seeds [4], inactivation of viruses in agriculture and food storage, wastewater treatment, etc. [5], spacecraft propulsion [6, 7], or VUV light emission [8, 9].

Because of all these beneficial uses, there has been a renewed interest in cold plasmas and, more generally, in non-thermal plasmas where the ions remain rather cold while electrons may be much hotter. A detailed understanding of their properties needed to develop new designs for their wide usage in common-life applications faces the necessity of microscopic data related to elementary processes occurring in non-thermal plasmas at the microscopic level. Specifically, collision cross-sections, charge exchange rates, mobility of ions under the influence of (often very strong) electric fields, thermal diffusion of ions, and others are needed. In this respect, numerical modeling and simulations play an irreplaceable role since experimental measurements are not always easily interpretable without the involvement of theory and/or cannot be easily performed at conditions that are hardly achievable in experiments but needed in modelings of extreme phenomena in cold plasma jets [10].

For some time, we have been involved in such studies aimed at the production of data needed for realistic macroscopic modelings of cold rare-gas plasmas inside plasma generators where rare-gas ions are produced and transported in the carrier gas. More specifically, during the last seven years, we have calculated transport properties and reaction rates of atomic (Rg^+) and

diatomic (Rg_2^+) ions of rare gases in the respective carrier rare gases (Rg), with Rg being helium, neon, argon, krypton, and xenon. A comprehensive overview of this effort can be found in summarizing works [11, 12] and references provided therein. Specifically, several studies were devoted to collision processes in cold helium plasma [13, 14]. In all these studies, the electronic interactions for the Rg_n^+ system rely on a very efficient *diatomics-in-molecules* modeling which requires only accurate *ab initio* inputs for the Rg_2^+ and Rg_2 diatomics. The next step towards a better understanding of the cold plasma active species and the efficiency of cold rare-gas plasmas in applications is clear. Namely, investigations of the interaction of the primary, rare-gas ions with the environment are needed. Naturally, such investigations must include, as a first step, calculations of the interaction of the primary ions with air, a primary environment component the plasma encounters after having left the inner space of a plasma generator, and its major part, molecular nitrogen (N_2), in particular.

Since the ionization potentials of rare gases are comparable (argon and heavier rare gases) or considerably higher (helium and neon) than the ionization potential of N_2, collisions resulting in charge transfer,

$$N_2 + Rg^+ \rightarrow N_2^+ + Rg, \tag{1}$$

represent a very first step on the route to the secondary and further plasma ions. Electronically excited states of the resulting N_2^+ ion will no doubt play a role due to the excess of energy released by the charge hop. Particularly for helium, the rare-gas with the highest ionization potential, production of electronically highly excited species (hereafter denoted by asterisk) is expected. These species may be either disintegrated due to an excess of internal energy,

$$N_2 + He^+ \rightarrow [N_2^+]^* + He \rightarrow [N^+]^* + N^* + He, \tag{2}$$

or quenched in subsequent collisions with cold constituents of the carrier gas,

$$N_2 + He^+ \rightarrow [N_2^+]^* + He \rightarrow \text{collisions} \rightarrow N_2^+ + He. \tag{3}$$

In all these processes, the N_2^+ ion appears either as a product or as an intermediate, i.e., a key ingredient of further reactions and transformations. Therefore, the interactions of the N_2^+ ion with the carrier rare gas must be well understood (and are thus worth to be in detail investigated) should the elementary collision events be described quantitatively correct.

While the charge-transfer processes of Eqs. (2) and (3) inherently include electronically highly excited states of the intermediate N_2^+ ion, the subsequent quenching collisions will produce the ion in its lower excited states or even in the electronic ground state. It is the main aim of the present work (as well as other studies which will follow from our group, see below) to thoroughly investigate the interactions of the N_2^+ ion in its electronic ground and lowest excited states with helium atoms. The question about the involvement of electronically highly excited N_2^+ ions in the early stages of the charge transfer process is postponed to a future work.

The N_2^+ (and therefore N_2^+/He) is known to be a very difficult system for *ab initio* approaches because of its intrinsic open shell and multiple bond nature where correlation effects are important. As there is no (semi)empirical model available for the N_2^+/He system, *ab initio* calculations are required. Advanced computational methods will thus be used starting from modeling of N_2^+/He electronic structure and potential energy surfaces using accurate *ab initio* methods (this paper), followed by dynamical calculations of N_2^+/He collisions and calculations of transport properties of the N_2^+ ion in helium buffer gas (prospective studies [15, 16]).

The main building unit of the N_2^+/He collision complex is the N_2^+ ion. Up to now, the ion has been intensively investigated in numerous experimental (see, e.g., [17, 18, 19, 20, 21, 22, 23]) and theoretical (see, e.g., [24, 25, 26, 27, 28, 29]) studies because of its great importance in atmospheric chemistry [30] and other research areas. From the point of view of *ab initio* calculations, the N_2^+ ion is a real challenge for the theory because of its inherently multi-reference nature, unpaired electrons, many energetically accessible shells, and extensive electronic correlations. Though the N_2^+/He complex has also been intensively studied both in theory and in experiment, reliable *ab initio* calculations leading to realistic potential energy surfaces [31, 32, 33] have been much less frequent than in the case of N_2^+. As a consequence, a thorough assessment of the methods to be eventually employed, for this composite ion, in dynamical calculations is of great importance.

The main focus of the present study is to perform a comprehensive series of such test calculations using various *ab initio* approaches in order to (mainly) assess the reliability of employed methods and their practicability in dynamical calculations reported in subsequent works of this series. Based on these tests, a decision on the level of the theory to be used in dynamical calculations as an acceptable trade-off between accuracy and computational demands will be made.

Following this introductory part, the rest of the paper is organized as follows. First, a brief overview of *ab initio* methods used in our calculations is given in section 2, then the main results we obtained are presented and discussed in section 3, specifically, the N_2^+ ion is investigated in section 3.1 and, then, the N_2^+/He complex is discussed in section 3.2. Finally, conclusive and summarizing remarks are provided in section 4.

2. Methods and computations

In this section, computational approaches used in the present work are described. Two classes of calculations are considered in sequence. First, the methods used to calculate the *potential energy curve*s (PECs) of the N_2^+ ion are discussed, then the approaches used in calculations of the *potential energy surface*s (PESs) of the N_2^+/He complex are outlined. Since mostly standard methods, which are well documented in the literature, have been used, only a brief summary is presented here. All the *ab initio* calculations reported in this work have been performed using the MOLPRO [34, 35] suite of codes, releases 2018.2.0 and 2021.1.

2.1. N_2^+ *calculations*

An extensive investigation of numerical aspects of the N_2^+ electronic structure calculations and their convergence has been performed since the ion represents, from the point of view of *ab initio* calculations, the most difficult part of the N_2^+/He complex. For both electronic states of the N_2^+ ion considered in this work, $X^2\Sigma_g^+$ and $A^2\Pi_u$, identical numerical settings and computational schemes have been used with specific steps considerably improving the convergence of performed calculations. As a first step, a *restricted Hartree-Fock* (RHF) calculation has been run for the (neutral) N_2 molecule. Then, state-specific calculations have been performed for the N_2^+ ion using a *multi-configuration self-consistent field* (MCSCF) method [36, 37]. Finally, the preceding calculations have been refined using a *multi-reference configuration interaction* (MRCI) [38, 39, 40] method.

Since the N_2^+ ion is a linear molecule, its symmetry is naturally described by the $D_{\infty h}$ point group. Considering that only Abelian groups are included in the MOLPRO package, the D_{2h} point group, the largest Abelian subgroup of $D_{\infty h}$, has been used for the linear N_2^+ ion. This subgroup has eight irreducible representations, A_g, B_{3u}, B_{2u}, B_{1g}, B_{1u}, B_{2g}, B_{3g}, and A_u, which

are used in this work to represent the symmetry of the N_2^+ electronic states instead of the commonly used *molecular orbital*s (MOs) notation.

The dependence of calculated PECs on employed *orbital space*s (OSs) have been investigated by considering the following cases: a) orbital space 1 (OS1) consisting of the minimal orbital space of the N_2^+ ion (comprising MOs $1a_g$, $1b_{1u}$, $2a_g$, $2b_{1u}$, $1b_{3u}$, $1b_{2u}$, $3a_g$, $1b_{2g}$, $1b_{3g}$, and $3b_{1u}$)[1] augmented, as proposed recently [28], with a b_{3u} MO, b) orbital space 2 (OS2) consisting of the minimal OS augmented with two more MOs resulting from 3s atomic orbitals (AOs) of the nitrogen atom ($4a_g$ and $4b_{1u}$), c) orbital space 3 (OS3) comprising the minimal OS augmented with the two MOs resulting from 3s AOs ($4a_g$ and $4b_{1u}$) and with two more bonding MOs resulting from $3p_{x,y}$ AOs ($2b_{3u}$ and $2b_{2u}$), and d) the most extensive orbital space 4 (OS4) with the minimal OS augmented with all the MOs resulting from all the 3s and 3p AOs of the nitrogen atom ($4a_g$, $4b_{1u}$, $2b_{3u}$, $2b_{2u}$, $5a_g$, $2b_{2g}$, $2b_{3g}$, and $5b_{1u}$)[2]. The lowest MOs ($1a_g$ and $1b_{1u}$) have been treated as "closed" in MCSCF calculations, i.e., always doubly occupied, and as "core" orbitals in MRCI calculations, i.e., doubly occupied and with their electrons not involved in excitations.

For these calculations, different augmented correlation-consistent basis sets of Dunning et al. [41] from triple through sextuple zeta cardinality, aug-cc-pVTZ (AVTZ), aug-cc-pVQZ (AVQZ), aug-cc-pV5Z (AV5Z), and aug-cc-pV6Z (AV6Z), have been considered.

The calculations have been performed over a dense grid of internuclear distances covering a range of $r = 0.7{-}15\,\text{Å}$ with a step of $\delta r = 0.01\,\text{Å}$ at short and medium distances (up to $r = 5\,\text{Å}$) and $\Delta r = 0.1\,\text{Å}$ in the long-distance region (up to $r = 15\,\text{Å}$). The infinite separation of the two nitrogen atoms, has been approximated by computations performed at internuclear distances of $r = 20, 50, 100\,\text{Å}$. A smooth representation of calculated points has been created, for each discrete PEC, for subsequent spectroscopic analysis. For example, the equilibrium distance in the N_2^+ ion, r_e, the ion binding energy, D_e, and its harmonic vibration frequency, ω_e, have been calculated using a cubic approximation of discrete PECs points in an immediate vicinity of the presumed PEC minimum. In each case, the point with the lowest

[1] $1\sigma_g$, $1\sigma_u$, $2\sigma_g$, $2\sigma_u$, $1\pi_x$, $1\pi_y$, $1\sigma_z$, $1\pi_x^*$, $1\pi_y^*$, $1\sigma_z^*$, and $2\pi_x$ in the standard MO notation, respectively.

[2] $3\sigma_g$, $3\sigma_u$, $2\pi_x$, $2\pi_y$, $2\sigma_z$, $2\pi_x^*$, $2\pi_y^*$, $2\sigma_z^*$

energy and eight more points around it have been used to get the PEC cubic representation via a least squares fit. Further, fully anharmonic vibrational energies have been calculated using a broader analytic representation of discrete PECs as implemented in the LEVEL16 software package [42]. First, a cubic spline has been calculated to interpolate discrete *ab initio* points. Note that the cubic splines have been applied to $r^2V(r)$ rather than to $V(r)$ itself on the repulsive wall of calculated potentials to get a more stable numerical behavior. The three points corresponding to the three largest distances considered ($r = 20, 50, 100\,\text{Å}$) have been used to adjust the long-range (LR) part of the potentials approximated by $V_{\text{LR}}(r) = V_{\text{asymp}} - \sum_{n=0}^{1} c_n/r^{4+2n}$.

Noteworthy, the spin-orbit coupling has not been considered in the present work since it is negligible compared to the accuracy achieved here for the N_2^+ ion (e.g., the spin-orbit splitting is of the order of $10\,\text{cm}^{-1}$ to $100\,\text{cm}^{-1}$ in N and N^+ [43]) and is completely out of game in He.

2.2. N_2^+/He *calculations*

As a second step, similar calculations have been performed for the N_2^+/He complex. Due to increased computational demands, as compared to the case of the N_2^+ ion, the calculations have been less extensive, however. Moreover, as mentioned above, the methodologically most involved part of the N_2^+/He complex is the inherently multi-configuration N_2^+ ion, and no dramatic change is expected in methodological complexity upon adding the helium atom until charge transfer between nitrogen and helium becomes important and, consequently, highly excited electronic states come into play[3]. For this reason, only a specific orbital space and a particular basis set have been considered in the N_2^+/He case. The particular choice (see below) has been made with regard to prospective dynamical calculations as a trade-off between computational costs and accuracy.

In line with the N_2^+ calculations, the three lowest electronic states of the N_2^+/He complex have been considered which asymptotically correlate to the $X^2\Sigma_g$ state and (doubly degenerate) $A^2\Pi_u$ state of the isolated N_2^+ ion. For the planar N_2^+/He complex, irreducible representations of the C_s group have been used to classify the electronic states of N_2^+/He, A' and A''. The lowest state of the A' symmetry (the ground state of the N_2^+/He complex)

[3]Since the ionization potential of the helium atom is by about 10 eV higher than that of N_2, the charge transfer between N_2^+ and He requires electronically highly excited N_2^+ ions.

asymptotically correlates to the $X^2\Sigma_g$ state of N_2^+, the first excited state of the A' symmetry and the lowest state of the A'' symmetry correspond to the doubly degenerate $A^2\Pi_u$ state of N_2^+.

An OS containing eleven a' MOs and two more a'' MOs has been used in the case of N_2^+/He calculations. It basically corresponds to OS2 introduced in the preceding subsection for the N_2^+ ion with a 1s orbital added for the helium atom. Having in mind the prospective dynamical calculations, their computational demands, and desired accuracy, an aug-cc-pVQZ(spdf) (AVQZ′) basis set has been used with only the *spdf* functions considered and the g functions omitted.

The general computational scheme adopted for the N_2^+/He complex comprises a couple of steps needed to get well-converged outputs. First, an RHF calculation has been run on the (neutral) N_2He complex with the minimal OS. Then, either a state-specific MCSCF calculation has been performed for the ion (N_2^+/He) in the case of the ground state calculation, or a three-state-averaged ($2\times A'+1\times A''$) MCSCF calculation for the first point followed by a series of two-state-averaged calculations for the other points (in the case of the $2A'$ calculations) or state-specific calculations (in the case of $1A''$ calculations) with the wave function ansatz taken from a preceding step. Note that the adopted scheme of calculations turned out to be essential for achieving an overall convergence in both the MCSCF method and its MRCI refinement (with points computed separately due to computational time, taking the wave function ansatz from the MCSCF step). Particularly, if the $2\times A'+1\times A''$ step is omitted, major convergence issues may be faced at the MRCI level.

A sufficiently dense grid of the Jacobi angle values[4] has been considered in order to well capture the anisotropy of the N_2^+/He PES, $\theta \in [0°, 90°]$ with $\Delta\theta = 15°$, and a broad range and sufficiently dense grid of Jacobi distances[5] have been used, $r = 0.7{-}5\,\text{Å}$ and $R = 0.7{-}5\,\text{Å}$ with $\Delta r = 0.1\,\text{Å}$ and $\Delta R = 0.1\,\text{Å}$, to get an extended and sufficiently detailed representations of the N_2^+/He PESs. In addition, asymptotic values of $r = 100\,\text{Å}$ and $R = 100\,\text{Å}$ have been added to assess the dissociation energy. Smooth representations of selected 1D and 2D cuts through the three N_2^+/He PESs considered in this work have been subsequently obtained using 1D and 2D cubic splines,

[4]The angle between the N_2^+ axis and the line connecting the He atom with the center-of-mass of the N_2^+ ion.

[5]The distance between the two N atoms, r, and the distance between the He atom and the center-of-mass of the N_2^+ ion, R

respectively, as implemented in the MATLAB software package [44].

3. Results and discussions

3.1. The N_2^+ ion

Before proceeding with the calculations of the PESs for the N_2^+/He collision complex, we performed some preliminary calculations on the N_2^+ ion. Our aim was to make a reasonable choice from both computational effort and accuracy points of view between different correlation methods, active spaces, and basis sets. For this, we will mainly concentrate on the comparison between MCSCF and MRCI approaches for different combinations of orbital spaces (see subsection 2.1 for description) and correlation consistent basis sets. As mentioned above, using purely MRCI potentials would be too time consuming for the subsequent dynamics studies, thus this comparison will serve as a calibration of the missing dynamical correlation using MCSCF potentials. For the same reason, core correlation is not taken into account in our calculations, leading to an expected underestimation of the dissociation energy of ~ 0.05 eV and an overestimation of the bond length and harmonic frequency of respectively 0.001 Å and ~ 10 wavenumbers [45].

3.1.1. The electronic ground state ($X\,^2\Sigma_g^+$)

The accurate computation of correlation effects for N_2^+ ion is known to be a very difficult problem. Usually, the larger the basis set and the larger the active space for the MRCI, the better are the results. However for N_2^+, as shown by Liu and coworkers [29] this is not systematically the case. This is also confirmed in the present work as can be seen in table 1 showing the dissociation energy of the ground state for different basis sets and active spaces. Indeed, at the MRCI level the dissociation energy for all the active spaces increases with the basis set while, for a given basis set, increasing the orbitals space results in a decrease of the bond energy. Compared to the most recent experimental value $D_e = 8.71$ eV [46], AVQZ′/OS2 seems to be a reasonable choice, moreover at a rather low computational cost. In this case, the difference between MCSCF and MRCI is only 3.7% with an absolute error of 0.321 eV. With this combination, the r_e for MCSCF and MRCI are 112.1 pm and 112.0 pm, respectively and the corresponding ω_e, 2193 and 2185 cm^{-1}, to be compared with the experimental values $r_e = 111.6$ pm and $\omega_e = 2207\,cm^{-1}$ [19].

Overall, the variations with the basis sets and active spaces are much smoother and we only report the differences between the MCSCF and MRCI calculations. figure 3 shows the evolution of the difference between MCSCF and MRCI spectroscopic constants. As can be seen, the trend with varying basis set is almost the same whichever active space is considered. Except for the smallest case, OS1, all the active spaces provide better result with increasing basis set. Again, AVQZ′/OS2 appears to be a good trade-off with very small deviations of the MCSCF results compared to the reference AV6Z/OS4 MRCI.

Difference between MCSCF and MRCI potential energy for the ground state is shown in figure 2 for the whole range of r. One can see a somewhat erratic behavior either when increasing the basis set or the active space (inset) due to a delicate interplay of static and dynamical correlation as well as size-consistency estimation. All the previous comparisons show that the MCSCF and MRCI PEC around the minimum present a rather similar shape. This similarity of the PECs is also reflected in the differences in the vibrational levels plotted in figure 3. Indeed, the differences are very small for the five lowest levels when using space OS2 and basis set AVQZ or larger. This difference grows slowly with v but remains low until $v = 15$. The discrepancy for the larger v is related to the error in the D_e already commented above. Even if the absolute errors may seem quite large in some cases ($\sim$500 cm^{-1}), the overall difference between MRCI and MCSCF results remain smaller than $2 - 3\%$ for the vibrational levels G_v.

3.1.2. The lowest excited state ($\mathrm{A}\,^2\Pi_u$*)*

In this section, we present the same set of results as above for the $\mathrm{A}\,^2\Pi_u$ state, which is another state of interest for the complex N_2^+/He . In table 2 we give the dissociation energy of the $\mathrm{A}\,^2\Pi_u$ state for different basis sets and active space sizes. The same trend as for the ground state can be seen here. Increasing the basis set deepens the potential well while the effect of the active space is less systematic, for instance, the MCSCF vs MRCI deviations are larger for OS3 than for OS2. Here again, it seems that AVQZ′/OS2 is a good trade-off also for this state.

The global behavior for r_e, ω_e and D_e reported in figure 4 is basically similar to what was obtained for the ground state. Again, the results are in favor of the AVQZ′/OS2 combination which compares well with the best estimation using AV6Z/OS4.

In figure 5, one can see that the energy difference between MCSCF and

MRCI globally decreases when the basis sets increase and presents a non uniform behavior with r with a small increase close to $r = 2.5\,\text{Å}$ and around the minimum. Like for the ground state, the green curve corresponding to the AVQZ′/OS2 set of calculation provides the overall best agreement between MCSCF and MRCI energies for all r.

figure 6 shows a monotonous variation of the difference of MCSCF and MRCI vibrational levels with v. Again, the best agreement with the reference calculations (AV6Z/glsos4, MRCI) is obtained for AVQZ′/OS2 combination.

3.1.3. Discussion of the N_2^+ *calculations*

To conclude this thorough comparison of different basis sets and active space for the ground state and the first excited state of the N_2^+ ion, it appears that AVQZ′/OS2 is a good candidate for a balanced description of all basic spectroscopic data at a reasonable computational cost. This is further illustrated by figures 7 and 8, where the AVQZ′/OS2 and the AV6Z/OS4 potential curves for the two lowest states are plotted. The global behavior is good and the curves are rather similar, although the bonding energy is slightly underestimated for the ground state ($X\,^2\Sigma_g^+$) and slightly overestimated for the excited state ($A\,^2\Pi_u$) at the MCSCF AVQZ′/OS2 level. Noteworthy, for both states the results for MCSCF AVQZ′/OS2 almost coincide with the ones for MRCI AV6Z/OS4. Thus, this reasonable choice will be used to perform dynamical calculations for the N_2^+/He complex using either on-the-fly MCSCF or neural network based potentials.

In figures 2 and 5, we show the difference between the MCSCF and MRCI potential energies for the $X\,^2\Sigma_g^+$ ground state and the $A\,^2\Pi_u$ lowest excited state, relative to dissociation. It is clear from these plots that OS1 and OS2 spaces (brown and blue curves, respectively) lead to significantly larger deviations than the OS3 active space using the same AV6Z basis set (red curve). Regardless of the basis set, OS3 results in quite close potential curves over a large range of interatomic distance, the maximum difference being $\lesssim 0.2\,\text{eV}$ for the ground state and less than $0.3\,\text{eV}$ for the excited state. This remains true already for the middle size AVQZ′ basis set at an expectedly reasonable computational cost for the N_2^+/He complex. The similarity of the potential curves is also reflected in the differences in the vibrational levels of the two states plotted in figures 3 and 6. In both cases, the differences are very small for the five lowest levels when using space OS3 and basis set AVQZ or larger. For the ground state, the difference grows slowly with v but remains very low until $v = 15$, showing that mainly the dissociation part

of the potential is affected by missing dynamical electron correlation. The same trend is true for the excited state but slightly worsened. Even if the absolute errors may seem quite large in some cases ($\sim$1000 cm^{-1}), the overall difference between MRCI and MCSCF results remain smaller than 2–3% for the vibrational levels G_v. The effect of increasing the active space on the spectroscopic constants r_e, D_e and ω_e is very small as can be seen in figures 1 and 4. At the MRCI level, the dissociation energy of the ground state obtained with the AVQZ basis set and active space OS3, 8.75 eV (see table 1), compares well with the most recent experimental value, $D_\mathrm{e} = 8.71$ eV [46], as do the $r_\mathrm{e} = 111.6$ pm and $\omega_\mathrm{e} = 2207\,\mathrm{cm}^{-1}$ spectroscopic constants [19]. This is also true for the A $^2\Pi_u$ state. The crucial point here is the size of the basis set as evidenced by significant discrepancies between the AVTZ and the other extended basis sets.

3.2. The N_2^+/He *collision complex*

Extending the N_2^+ calculations reported in the preceding subsection, we have also performed similar calculations for the N_2^+/He complex with the main focus on checking the accuracy of MCSCF and MRCI approaches in the case of this more involved system. To save computational time, only the AVQZ′/OS2-like approach (see subsection 2.2), which has proved its quality in the N_2^+ calculations of the preceding subsection, has been used without any aim of a detailed convergence analysis like that performed for the N_2^+ ion.

In figure 9, we show the MRCI and MCSCF PESs for selected cuts of the potential energy surface for different approaching angles. In all cases, for short He$-N_2^+$ distances the MRCI curve is less repulsive than the MCSCF one due to the better inclusion of dynamical correlation between He and N_2^+ electrons. In table 4, we give the minima of the ground state potential curve for the MCSCF and MRCI calculations. For sake of comparison with previous calculations, we also give the He$-N_2^+$ distance and corresponding dissociation energy for the typical T-shaped and $\theta = 45°$ geometries. In all cases, the N_2^+ distance was kept equal to its equilibrium value ($r_\mathrm{e} = 2.11$ a.u. ≈ 1.117 Å). We can see, that our MRCI results are very close to previous calculations [10, 32, 33]. As can be seen in table 4, in our calculation, the minimum was found for geometries close to an approaching angle of 45° as was the case in the MCSCF-CI study by Miller *et al.* [31], but differs from the calculation of Guillon and Stoecklin [33] who found the T-shaped form as the most stable structure. We may also note that, that for 90° the latter

obtained a shallower potential well. Unfortunately, these authors do not give sufficient computational details to assess the origin of this discrepancy. The wells' depths are so close to each other, that this sensitivity may result from different multi-reference treatment or different basis sets. For both excited states in A' and A'' symmetries, we found the minimum at 90° as in a reference [32] with very similar characteristics.

Going much beyond all the previous studies, we have performed explorations of the PES not only around the minimum but also in a much wider range to have an idea of their global behavior and test their sensitivity to the most interesting *ab initio* approaches previously considered for N_2^+. Some representative cuts of the ground-state PESs of the N_2^+/He ion at a fixed angle corresponding to N_2^+/He equilibrium geometry (θ_e) are given in figures 10 and 11 for MCSCF and MRCI, respectively. In both figures, the minimum area is magnified in the inset. Along the He$-N_2^+$ distance (R) there is a rather flat behavior, however at very high energy around 8000 meV we see the start of the exit recombination channel $HeN^+ + N$. The global shape is similar for both MCSCF and MRCI potentials, although the minimum of HeN^+ MRCI valley looks slightly shifted to smaller R distances. This is in accordance with our comment of figure 9. For both excited states, as can be seen in figures 12, 13, 14 and 15, the global behavior is very similar between MCSCF and MRCI again with a shallow minimum along R. The main difference is that, for both excited states, MRCI leads to a slightly deeper well, at slightly shorter R.

Having all that in mind, we conclude that the MCSCF/AVQZ′/OS2 method represents, from the point of view of subsequent dynamical calculations, an acceptable trade-off between computational demands and accuracy. To further support this choice, we have thoroughly analyzed the computational costs of MCSCF and MRCI methods (employed at the AVQZ′/OS2 level). It follows from this analysis, that for the MOLPRO version used in the present work and for the computers on which the calculations were run (equipped with 2.6 GHz AMD 7H12 processors with totally 128 CPU cores and 256 GB of RAM per computational node), typically about 45 seconds are needed to evaluate the interaction energy of N_2^+/He and its gradients in a single ion configuration if MOLPRO is run in the serial mode (i.e., without any parallelization)[6]. From the point of view of the prospective dynamical

[6]It further follows from our calculations that if a parallel version of the MOLPRO

calculations, for which typically thousands of trajectories are needed, each comprising (in dependence on the collision energy) hundreds to thousands integration steps, altogether dozens of thousands of core-hours will be needed to get converged collision data (cross-sections) for a particular collision energy, a rather acceptable demand if modern supercomputers are used. The situation would be, on the other hand, dramatically less favorable if the MRCI method were used. At the same level of accuracy (AVQZ′/OS2), a single-point calculation (performed in the serial regime) requires about 90–100 hours for low collision energies ($E_{\mathrm{coll}} \approx 0.01\,\mathrm{eV}$) and this number decreases down to about 5–10 hours in the high collision energy region ($E_{\mathrm{coll}} \approx 50$–$100\,\mathrm{eV}$). Resulting demands of dynamical calculations will thus rise as high as several millions or even several dozens of millions core-hours per collision energy. While such demands are still acceptable for the presently available supercomputers, related wall times amounting up to dozens or even hundreds of days are not.

4. Conclusions

PESs of the N_2^+ ion in its electronic ground state ($X\,^2\Sigma_g^+$) and the lowest excited state ($A\,^2\Pi_u$) have been calculated using *multi-configuration self-consistent field* (MCSCF) and *multi-reference configuration interaction* (MRCI) with a detailed focus on the convergence of calculations with atomic basis set and orbital space used. A broad range of Dunning's correlation consistent basis sets (aug-cc-pVXZ, AVXZ, X = T,Q,5,6) [41] has been considered as well as orbital spaces covering the minimal orbital space ($1\sigma_g 1\sigma_u 2\sigma_g 2\sigma_u 2\pi_u 2\pi_g 3\sigma_g 3\sigma_u$) augmented by a $3\pi_u$ function as proposed in Ref. [28], by a pair of $4\sigma_g$ and $4\sigma_u$ functions resulting from $3s$ atomic orbitals, and, finally, augmented by functions $4\sigma_g$, $4\sigma_u$, $3\pi_u$, $3\pi_g$, $5\sigma_g$, and $5\sigma_u$ resulting from both $3s$ and $3p$ atomic orbitals. **The MCSCF method has been mainly selected as a trade-off between sufficient accuracy and computational practicability of subsequent calculations focused on the dynamics of N_2^+/He collisions (including, e.g., analytical gradients implemented for the**

code is used with 4 CPU cores involved, the single-point time decreases down to about 18 sec, which means that a reduction of about 2.6 times may be achieved in the wall-time. However, if the total consumption of computational resources (expressed in consumed core-hours) is considered, the parallel, four-core calculation is about 1.5 times less efficient than the single-core one. For this reason, we decided to employ the MOLPRO code in the serial regime in subsequent dynamical calculations.

method in external software packages to avoid lengthy numerical calculations of inter-atomic forces.)

The potential energy curves have been used to calculate basic spectroscopic constants of the N_2^+ ion (R_e, D_e, and ω_e) and lowest vibrational energies ($G(v), v \leq 29$), for which the convergence with basis set and orbital space has been investigated in detail. A thorough comparison with selected experimental studies [17, 19, 18, 20, 21, 23, 22] as well as the most recent theoretical calculations [28, 29] has been performed. Moreover, the performance of the MCSCF method, as a computationally cheap alternative for on-the-fly electronic structure calculations in, e.g., dynamical simulations, has also been assessed by comparing with reference MRCI data.

In general, a smooth and monotonous convergence of the calculated data has been achieved with both increased cardinality of the basis set and increased size of the orbital space, both for the $X\,^2\Sigma_g^+$ state and the $A\,^2\Pi_u$ state. Most importantly, a very good correspondence with available experiments and recent calculations has been obtained for the MCSCF method and moderate basis sets. as compared with reference MRCI/AV6Z calculations. For example, the computationally cheapest MCSCF/AVTZ calculation has led to an encouraging accuracy with the MRCI value of D_e reproduced within about 1.5% – 3.1% and with the accuracy achieved for R_e and/or ω_e being even much better (about 1% and less).

For the triatomic system, N_2^+/He, we have studied three lowest electronic states dissociating to the ground state and the Π state of N_2^+, the ground and the first excited state in symmetry A' and the lowest state in symmetry A''. Beyond the determination of the minimum, the PESs have been explored for a wide range of Jacobi distances and a dense grid of selected Jacobi angles. As for N_2^+ an encouraging agreement between specific MCSCF and large MRCI results has been found. Moreover, the adopted MCSCF approach leads to a very good agreement with N_2^+/He mobility measurements if used together with a moderate basis set (AVQZ′) and employed on-the-fly in subsequent dynamical calculations [15] and Monte Carlo modelings [16] of the N_2^+/He complex. It thus seems that the electronic structure effects not properly taken into account in the adopted *ab initio* approach based on the MCSCF method do not much affect the N_2^+/He collision dynamics,**except for very low collision energies [15], about and below 0.01 eV. For these energies, the contribution of missing dynamical electronic correlation in MCSCF is important and may lead to observable differences between theoretical and experimental esti-**

mates of N_2^+/He collision cross-sections [15]. However, such very low collision energies are not crucial at typical experimental conditions ($T = 300\,\mathbf{K}$) even if weak electric fields are considered [16]. To avoid unnecessary lengthening of the present paper, the reader is referred for a full discussion of the subsequent calculations to the cited studies [15, 16]. The effect of the correlation energy in low-energy N_2^+/He collisions is thus still not fully resolved. One possibility to overcome this difficulty may be to use some multi-reference perturbative approach or the benchmark, MRCI method in the dynamical calculations. In future work, feasibility of on-the-fly MRPT2 calculations will be tested and compared to neural network fitted MRCI potential energy curves.

The present work focuses on a detailed estimation of accuracy of various approaches to electronic structure calculations on the N_2^+ and N_2^+/He ions, the first step to well-controlled simulations of collision dynamics of N^+ and N_2^+ ions with rare-gas atoms which represent an important class of elementary collision occurring in low-temperature atmospheric-pressure rare-gas plasmas. As such, it should help to get reliable numerical data on these collision processes and is expected to contribute considerably to running theoretical research on cold rare-gas plasmas and their properties. In forthcoming works, the present *ab initio* studies will be used to estimate the dynamics of N_2^+/He collisions and cross sections [15] and resulting transport properties of N_2^+ in He [16]. **Another interesting question which deserves a thorough consideration is about the effect electronic excitations have on the dynamics of N_2^+/He collisions. Calculations addressing this principal problem are being presently prepared in our group. An approximately diabatic interaction model including the lowest electronic states of the N_2^+/He ion ($2 \times A' + A''$) proposed in Ref. [32] and asymptotically correlating to the $X\,^2\Sigma_g^+$ and $A\,^2\Pi_u$ states of the N_2^+ ions will be used and build up on the results obtained within the present work.**

Acknowledgments

The work has been supported by the Ministry of Education, Youth and Sports of the Czech Republic via the *National Programme of Sustainability II*, project *IT4Innovations excellence in science* (grant no. LQ1602), and the *e-INFRA CZ* project (grant no. ID:90140). The calculations have been

performed on the supercomputers of the *IT4Innovations* National Supercomputing Center which have been made available to us through computational grants OPEN-23-12, OPEN-22-21, OPEN-21-46, OPEN-20-34, OPEN-17-50, OPEN-17-15, OPEN-16-14, OPEN-16-3, OPEN-14-25, OPEN-11-4, and DD-20-23.

References

[1] M. Laroussi. Low-temperature plasmas for medicine? *IEEE Trans. Plasma Sci.*, 37(6):714, June 2009.

[2] M. Yousfi, N. Merbahi, A. Pathak, and O. Eichwald. Low-temperature plasmas at atmospheric pressure: toward new pharmaceutical treatments in medicine. *Fund. Clin. Pharm.*, 28(2):123, February 2014.

[3] H. Tanaka, K. Ishikawa, M. Mizuno, S. Toyokuni, M. Kajiyama, F. Kikkawa and. H.-R. Metelmann, and M. Hori. State of the art in medical applications using non-thermal atmospheric pressure plasma. *Rev. Mod. Plasma Phys.*, 3(1):1, July 2017.

[4] M. Bafoil, A. Jemmat, Y. Martinez ans N. Merbahi, O. Eichwald, C. Dunand, and M. Yousfi. Effects of low temperature plasmas and plasma activated waters on arabidopsis thaliana germination and growth. *PLoS ONE*, 13(4):4, April 2018.

[5] A. Filipić, G. Primc, R. Zaplotnik, N. Mehle, I. Gutierrez-Aguirreand M. Ravnikar, M. Mozetič, J. Žel, and D. Dobnik. Cold atmospheric plasma as a novel method for inactivation of potato virus y in water samples. *Food Env. Virol.*, 11:220, 2019.

[6] A. I. Bugrova, A. M. Bishaev, A. V. Desyatskov, M. V. Kozintseva, A. S. Lipatov, and M. Dudeck. Experimental investigations of a krypton stationary plasma thruster. *Int. J. of Aero. Eng.*, 2013:ID 686132, 2013.

[7] S. Mazouffre. Electric propulsion for satellites and spacecraft: established technologies and novel approaches. *Plasma Sources Sci. Technol.*, 25(3):033002, April 2016.

[8] N. Merbahi, G. Ledru, N. Sewraj, and F. Marchal. Electrical behavior and vacuum ultraviolet radiation efficiency of monofilamentary xenon dielectric barrier discharges. *J. Appl. Phys.*, 101(12):123309, June 2007.

[9] P. Muranyi, J. Wunderlich, and M. Heise. Sterilization efficiency of a cascaded dielectric barrier discharge. *J. Appl. Microbiol.*, 103(5):1535, June 2007.

[10] M. Yousfi, A. Hennad, M. Benhenni, O. Eichwald, and N. Merbahi. Basic data of ions in He-air mixtures for fluid modeling of low temperature plasma jets. *J. Appl. Phys.*, 112(4):043301, August 2012.

[11] A. Chicheportiche. *Basic data of atomic and molecular helium and argon ions for the optimization of low temperature plasma jets used in the biomedical field.* PhD thesis, Université Toulouse III Paul Sabatier, 2014. in French.

[12] C. Van de Steen. *Modeling of transport properties of ions of krypton and xenon for optimization of cold rare-gas plasmas generators.* PhD thesis, Université Toulouse III Paul Sabatier and VSB – Technical University of Ostrava, 2018.

[13] A. Chicheportiche, B. Lepetit, M. Benhenni, F. X. Gadea, and M. Yousfi. Ab initio transport coefficients of Ar^+ ions in Ar for cold plasma jet modeling. *Phys. Rev. E*, 89(6):063102, jun 2014.

[14] A. Chicheportiche, B. Lepetit, M. Benhenni, F. X. Gadea, and M. Yousfi. Comparative study of collision cross-sections and ion transport coefficients from several He^+/He interaction potentials. *J. Phys. B: At. Mol. Opt. Phys.*, 46(6):065201, feb 2013.

[15] S. Paláček, M. Beseda, R. Kalus, M. Benhenni, M. Yousfi, T. Leininger, and F. X. Gadéa. Modeling of the N_2^+ ion in cold helium plasma: dynamics of N_2^+/he collisions and cross-sections. Submitted to Plasma Source Sci. Tech.

[16] S. Paláček, M. Beseda, R. Kalus, M. Benhenni, M. Yousfi, T. Leininger, and F. X. Gadéa. Modeling of the N_2^+ ion in cold helium plasma ii: transport properties of N_2^+ in helium. under preparation.

[17] F. R. Gilmore. Potential energy curves for N_2, NO, O_2, and corresponding ions. *J. Quant. Spec. Rad. Trans.*, 5:369, 1965.

[18] Alf Lofthus and Pual. H. Krupenie. The spectrum of molecular nitrogen. *J. Phys. Chem. Ref. Data*, 6:113, 1977.

[19] K. P. Huber and G. Herzberg. *Molecular Spectra and Molecular Structure IV. Constants of Diatomic Molecules*. Litton Educational Publishing Inc., New York, 1979.

[20] R. A. Gottscho, R. W. Field, K. A. Dick, and W. Benesch. Deperturbation of the N_2^+ First Negative Group $B^2\Sigma_u^+ - X^2\Sigma_g^+$. *J. Mol. Spec.*, 74:435, 1979.

[21] L. Klynning and P. Pagès. The band spectrum of N_2^+. *Phys. Scr.*, 25:543, 1982.

[22] F. R. Gilmore, R. R. Laher, and P. J. Espy. Franck–condon factors, r-centroids, electronic transition moments, and einstein coefficients for many nitrogen and oxygen band systems. *J. Phys. Chem. Ref. Data*, 21:1005, 1992.

[23] T. J. Scholl, R. A. Holt, and S. D. Rosner. Fine and hyperfine structure in $^{14}N_2^+$: The $B^2\Sigma_u^+ - X^2\Sigma_g^+$ $(0,0)$ band. *J. Mol. Spec.*, 192:424, 1998.

[24] E. W. Thulstrup and A. A. Andersen. Configuration interaction studies of bound, low-lying states of N_2^-, N_2, N_2^+ and N_2^{2+}. *J. Phys. B: At. Mol. Phys.*, 8:965, 1975.

[25] S. R. Langhoff and C. W. Bauschlicher Jr. Theoretical study of the first and second negative systems of N_2^+. *J. Chem. Phys.*, 88:329, 1988.

[26] R. Polák and J. Fišer. A casscf/icmrci study of the electric field gradient in low-lying electronic states of N_2^+/N_2. *Chem. Phys.*, 290:177, 2003.

[27] M. Fehér and P. A. Martin. Ab initio calculation of the electrical properties of the $X^2\Sigma_g^+$ ground and $A^2\Pi_u$ excited states of N_2^+. *J. Chem. Soc. Far. Trans.*, 7:1063, 1995.

[28] Deheng Shi, Wei Xing, Jinfeng Sun, Zunlue Zhu, and Yufang Li. Spectroscopic constants and molecular properties of $X^2\Sigma_g^+$, $A^2\Pi_u$, $B^2\Sigma_u^+$ and $D^2\Pi_g$ electronic states of the N_2^+ ion. *Comp. Theor. Chem.*, 966:44, 2011.

[29] Hiu Liu, Deheng Shi, Shuai Wang, Jinfeng Sun, and Zunlue Zhu. Theoretical spectroscopic calculations on the 25 λ–s and 66 ω states of N_2^+ cation in the gas phase including the spin–orbit coupling effect. *J Quant Spectrosc Radiat Transf*, 147:207, 2014.

[30] D. M. Hunten. The production of N_2^+ in the atmosphere. *Planet. Space Sci.*, 10:37–45, 1963.

[31] Steven Miller, Jonathan Tennyson, Bernd Follmeg, Pavel Rosmus, and Hans-Joachim Werner. Ab initio investigation of the bound rovibrational states in the electronic ground state of HeN_2^+. *J. Chem. Phys*, 89(4):2178–2184, 1988.

[32] Andreas Berning and Hans-Joachim Werner. Quantum scattering studies of electronically inelastic collisions of $N_2^+(X^2\Sigma_g^+, A^2\Pi_u)$ with He. *J. Chem. Phys.*, 100(3):1953–1967, 1994.

[33] G. Guillon and T. Stoecklin. A comparative nearside-farside analysis of the $He - N_2^+$ and $He - N_2$ inelastic collisions. *Eur. Phys. J. D*, 39(3):359–371, 2006.

[34] H.-J. Werner, P. J. Knowles, G. Knizia, F. R. Manby, and M. Schütz. Molpro: A general-purpose quantum chemistry program package. *WIREs Comput. Mol. Sci.*, 2(2):242–253, July 2012.

[35] H.-J. Werner, P. J. Knowles, G. Knizia, F. R. Manby, M. Schütz, et al. MOLPRO, version 2019.2, a package of ab initio programs, 2019.

[36] Hans-Joachim Werner and Peter J. Knowles. A second order multiconfiguration scf procedure with optimum convergence. *J. Chem. Phys.*, 82(11):5053–5063, 1985.

[37] Peter J. Knowles and Hans-Joachim Werner. An efficient second-order MC SCF method for long configuration expansions. *Chem. Phys. Lett.*, 115(3):259–267, 1985.

[38] Hans-Joachim Werner and Peter J. Knowles. An efficient internally contracted multiconfiguration–reference configuration interaction method. *J. Chem. Phys.*, 89(9):5803–5814, 1988.

[39] Peter J. Knowles and Hans-Joachim Werner. An efficient method for the evaluation of coupling coefficients in configuration interaction calculations. *Chem. Phys. Lett.*, 145(6):514–522, 1988.

[40] Peter J. Knowles and Hans-Joachim Werner. Internally contracted multiconfiguration–reference configuration interaction calculations for excited states. *Theor. Chim. Acta*, 84(1-2):95–103, 1992.

[41] Kirk A. Peterson and Thom H. Dunning Jr. Accurate correlation consistent basis sets for molecular core–valence correlation effects: The second row atoms Al–Ar, and the first row atoms B–Ne revisited. *J. Chem. Phys.*, 117(23):10548–10560, 2002.

[42] Robert J. Le Roy. LEVEL: A computer program for solving the radial schrödinger equation for bound and quasibound levels. *J Quant Spectrosc Radiat Transf*, 186:167–178, January 2017. Satellite Remote Sensing and Spectroscopy: Joint ACE-Odin Meeting, October 2015.

[43] Charlotte E Moore. Selected Tables of Atomic Spectra, Atomic Energy Levels. Multiplet Tables N I, N II, N III. Technical report, NATIONAL STANDARD REFERENCE DATA SYSTEM, 1975.

[44] MATLAB 9.9.0.1857802 (R2020b) Update 7. 2020.

[45] A. G. Császár and W. D. Allen. The effect of 1s correlation on d_e, r_e , and ω_e of first-row diatomics. *J. Chem. Phys.*, 104:2746–2748, 1996.

[46] Xiaonan Tang, Yu Hou, C. Y. Ng, and Branko Ruscic. Pulsed field-ionization photoelectron-photoion coincidence study of the process $N_2 + h\nu \rightarrow N^+ + N + e^-$: Bond dissociation energies of N_2 and N_2^+. *J. Chem. Phys*, 123(7):074330, August 2005.

[47] K. Ohtsuki, M. Hananoe, and M. Matsuzawa. Anomalous decline of molecular ion mobility in cooled helium gas. *Phys. Rev. Letters*, 95:213201, 2005.

[48] T. Schmelz, P. Rosmus, A. Berning, and H. J. Werner. Bound rovibronic levels of the $HeN_2^+(A^2\Pi)$ complex. *Spectrochimica Acta A*, 53:1133, 1997.

[49] H. W. Ellis, R. Y. Pai, E. W. McDaniel, E. A. Mason, and L. A. Viehland. Transport properties of gaseous ions over a wide energy range. *At. Data Nucl. Data Tables*, 17(3):177, March 1976.

Tables

Table 1: Dissociation energies for the $X\,^2\Sigma_g^+$ state of the N_2^+ ion as obtained from MCSCF (D_e^{MCSCF}) and MRCI (D_e^{CI}) calculations and absolute ($\delta D_e \equiv D_e^{MCSCF} - D_e^{CI}$) and relative ($\delta_r D_e \equiv \delta D_e / D_e^{CI}$) differences between them. The last line (denoted by "T-6") in each section contains the differences between the cheapest, MCSCF /AVTZ, and the most accurate, MRCI/AV6Z, results. For OS2, the difference between MCSCF /AVQZ′ and MRCI/AV6Z is also added (line "Q′-6") for comparison. All the energies are given in eV.

basis	D_e^{MCSCF}	D_e^{CI}	δD_e	$\delta_r D_e$
orbital space 1 (OS1)				
AVTZ	9.153	8.656	0.497	+5.7 %
AVQZ	9.208	8.860	0.348	+3.9 %
AV5Z	9.213	8.920	0.293	+3.3 %
AV6Z	9.214	8.944	0.270	+3.0 %
T-6			0.209	+2.3 %
orbital space 2 (OS2)				
AVTZ	8.976	8.608	0.368	+4.3 %
AVQZ′	9.023	8.702	0.321	+3.7 %
AVQZ	9.033	8.817	0.216	+2.5 %
AV5Z	9.038	8.877	0.16	+1.8 %
AV6Z	9.039	8.901	0.137	+1.5 %
Q′-6			0.122	+1.2 %
T-6			0.075	+0.8 %
orbital space 3 (OS3)				
AVTZ	9.169	8.599	0.570	+6.6 %
AVQZ	9.247	8.811	0.436	+5.0 %
AV5Z	9.254	8.872	0.382	+4.3 %
AV6Z	9.255	8.896	0.359	+4.0 %
T-6			0.273	+3.1 %
orbital space 4 (OS4)				
AVTZ	8.960	8.543	0.418	+4.9 %
AVQZ	9.026	8.754	0.273	+3.1 %
AV5Z	9.031	8.815	0.217	+2.5 %
AV6Z	9.033	8.839	0.195	+2.2 %
T-6			0.121	+1.4 %

Table 2: The same as in table 1 but for the the A $^2\Pi_u$ electronic state of the N_2^+ ion.

basis	D_e^{MCSCF}	D_e^{CI}	δD_e	$\delta_r D_e$
orbital space 1 (OS1)				
AVTZ	8.037	7.554	0.483	+6.4 %
AVQZ	8.085	7.747	0.337	+4.4 %
AV5Z	8.089	7.805	0.284	+3.6 %
AV6Z	8.090	7.829	0.261	+3.3 %
T-6			0.208	+2.6 %
orbital space 2 (OS2)				
AVTZ	7.953	7.519	0.435	+5.8 %
AVQZ′	7.996	7.601	0.395	+5.2 %
AVQZ	8.004	7.712	0.292	+3.8 %
AV5Z	8.008	7.77	0.238	+3.1 %
AV6Z	8.009	7.793	0.216	+2.8 %
Q′-6			0.203	+2.6 %
T-6			0.160	+2.0 %
orbital space 3 (OS3)				
AVTZ	8.255	7.519	0.736	+9.8 %
AVQZ	8.316	7.715	0.601	+7.8 %
AV5Z	8.314	7.778	0.536	+6.9 %
AV6Z	8.315	7.802	0.513	+6.6 %
T-6			0.453	+5.8 %
orbital space 4 (OS4)				
AVTZ	7.939	7.466	0.473	+6.3 %
AVQZ	8.000	7.661	0.340	+4.4 %
AV5Z	8.005	7.720	0.285	+3.7 %
AV6Z	8.006	7.744	0.262	+3.4 %
T-6			0.195	+2.5 %

Table 3: Comparison of dissociation energy (ΔD_e) and equilibrium distance between the center-of-mass of the N_2^+ ion and the He atom (R_e) calculated for the electronic ground state ($1A'$) of N_2^+/He and for selected Jacobi angles (θ) and using different levels of *ab initio* calculations. The distance of atoms in N_2^+ has been fixed in all calculations at $r = 2.11$ bohr (≈ 1.117 Å). If not specified otherwise, data obtained within the present work are presented. The data reported for reference [47] have been extracted from figure 1 of that reference. Distances and binding energies are given in Å and meV, respectively.

	$\theta = 0°$		$\theta = 45°$		$\theta = 90°$	
method	R_e	ΔD_e	R_e	ΔD_e	R_e	ΔD_e
MCSCF	3.400	11.8	3.226	12.2	3.088	11.4
MRCI	3.227	19.3	3.034	20.1	2.879	19.2
MRCI [31]	3.280	16.5	3.090	17.3	2.799	16.7
MRCI [32][1]	3.265	17.2	–	–	2.910	17.2
MRCI [32][2]	3.291	17.4	–	–	2.948	15.8
MRCI [47]	3.262	18.6	3.069	19.3	2.899	18.3
MRCI [33]	–	–	–	–	3.217	10.5

[1] diabatic potential, equation (13) of reference [32]

[2] vibrationally adiabatic potential, equation (14) of reference [32]

Table 4: Comparison of the N_2^+/He $\rightarrow$ N_2^+ +He dissociation energy (ΔD_e) and corresponding equilibrium values of internal coordinates of the N_2^+/He ion obtained from different *ab initio* calculations. If not specified otherwise, the values obtained within the present work using the MCSCF/AVQZ′ method are presented. The values given for reference [32], ground state, have been extracted from figure 2 of that reference and ΔD_e represents a lower estimate of the true value, the values provided for the same reference for the two excited states have been taken from reference [48]. The IM value of ΔD_e corresponds to the depth of an effective N_2^+/He interaction potential derived from measured mobility of the N_2^+ ion in helium [49] in reference [10]. Angles, distances, and binding energies are given in degrees, Å, and meV, respectively.

method	θ_e	R_e	r_e	ΔD_e
ground state (1A′)				
MCSCF	49	3.209	1.122	12.1
MRCI	52	2.999	1.120	20.3
MRCI [32]	51	3.064	1.117[1]	$\gtrsim$ 17.9
MRCI [33]	90	3.217	1.117[1]	10.5
IM [10]				17.3
excited state (2A′)				
MCSCF	90	2.724	1.180	21.7
MRCI	90	2.476	1.178	38.9
MRCI [32]	90	2.500	1.117[1]	36.9
excited state (1A″)				
MCSCF	90	3.144	1.179	11.2
MRCI	90	3.009	1.178	18.0
MRCI [32]	90	2.949	1.117[1]	17.0

[1] fixed at $r_e = 2.11$ bohr

Figures

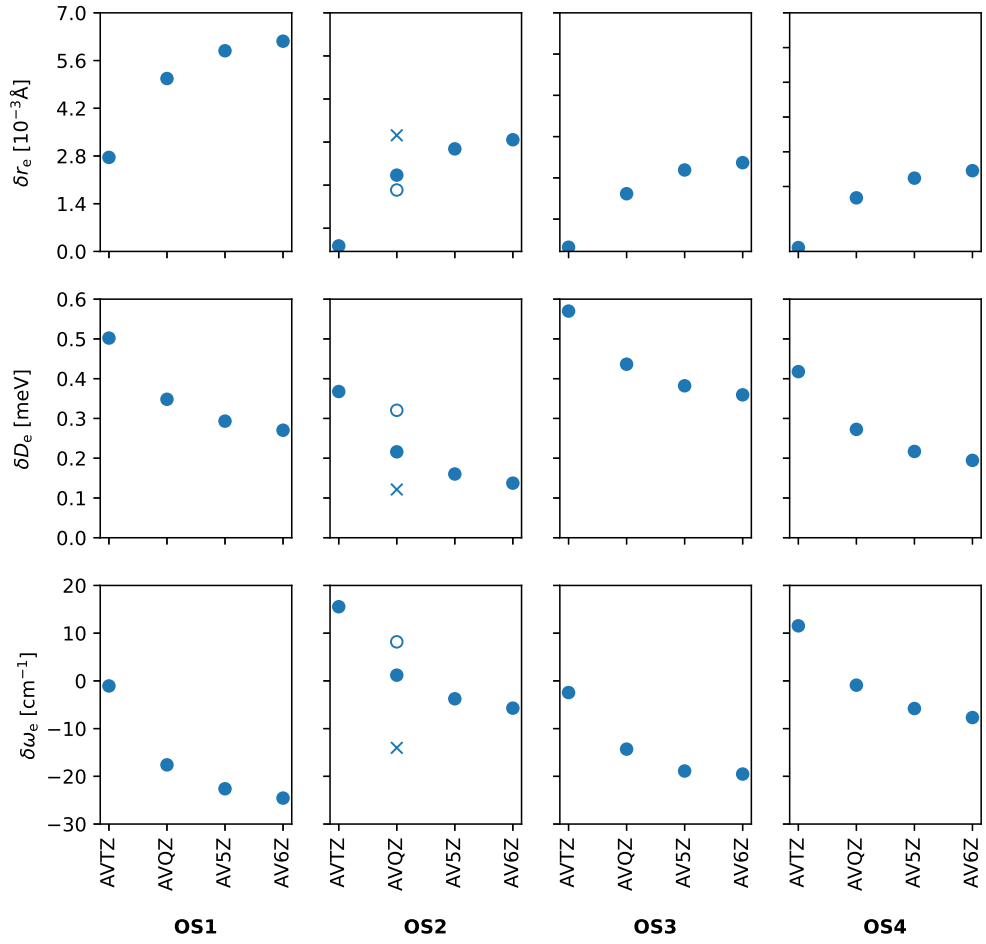

Figure 1: Differences of the N_2^+ binding energy, D_e, bond length, r_e, and harmonic vibrational frequency, ω_e as obtained for the $X\,^2\Sigma_g^+$ state of the ion from MCSCF and MRCI calculations (MCSCF −MRCI). Full dots correspond to calculations performed using the same basis set for both MCSCF and MRCI, open dots in the OS2 panels represent, for comparison, differences obtained for the AVQZ′ basis set, and crosses are used to show differences of MCSCF /AVQZ′−MRCI/AV6Z.

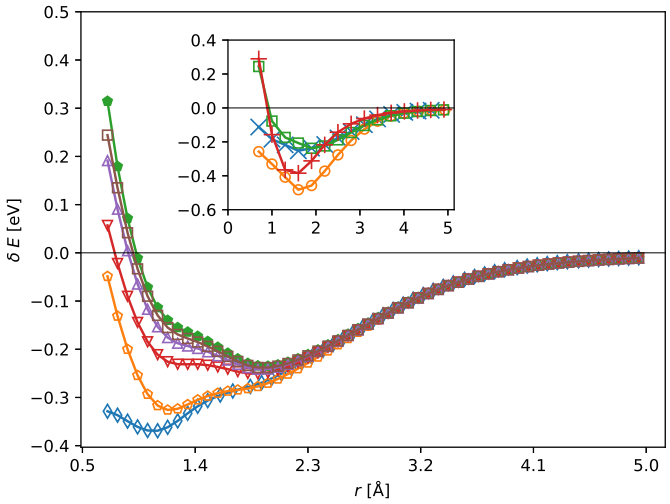

Figure 2: Differences between MCSCF and MRCI calculations (MCSCF −MRCI) performed for the $X\,^2\Sigma_g^+$ state of the N_2^+ ion at the OS2 level: diamonds/blue AVTZ, down triangles/red AVQZ, up triangles/violet AV5Z, and squares/brown AV6Z. Values obtained for the AVQZ′ basis set (empty pentagons/orange)and difference with MRCI/AV6Z (full pentagons/green) are also shown for comparison. In the inset, the evolution of calculated differences with the orbital space is shown as obtained for the largest basis set used in this work (AV6Z): pluses OS1, squares OS2, circles OS3, and times OS4. All the energies are set to zero as r approaches infinity.

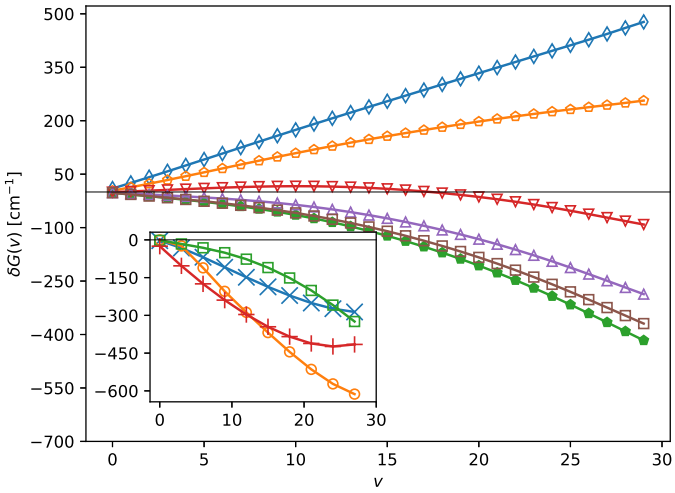

Figure 3: Differences between MCSCF and MRCI calculations (MCSCF −MRCI) of the lowest vibrational levels of N_2^+ performed for the $X\,^2\Sigma_g^+$ state of the ion. The symbols used are the same as in figure 2; the main panel: diamonds AVTZ, down triangles AVQZ, up triangles AV5Z, and squares AV6Z, empty pentagons AVQZ′, and full pentagons differences between MCSCF /AVQZ′ and MRCI/AV6Z (with all the calculations performed for the OS2 orbital space); the inset: pluses OS1, squares OS2, circles OS3, and times OS4 (with all the calculations performed for the AV6Z basis set).

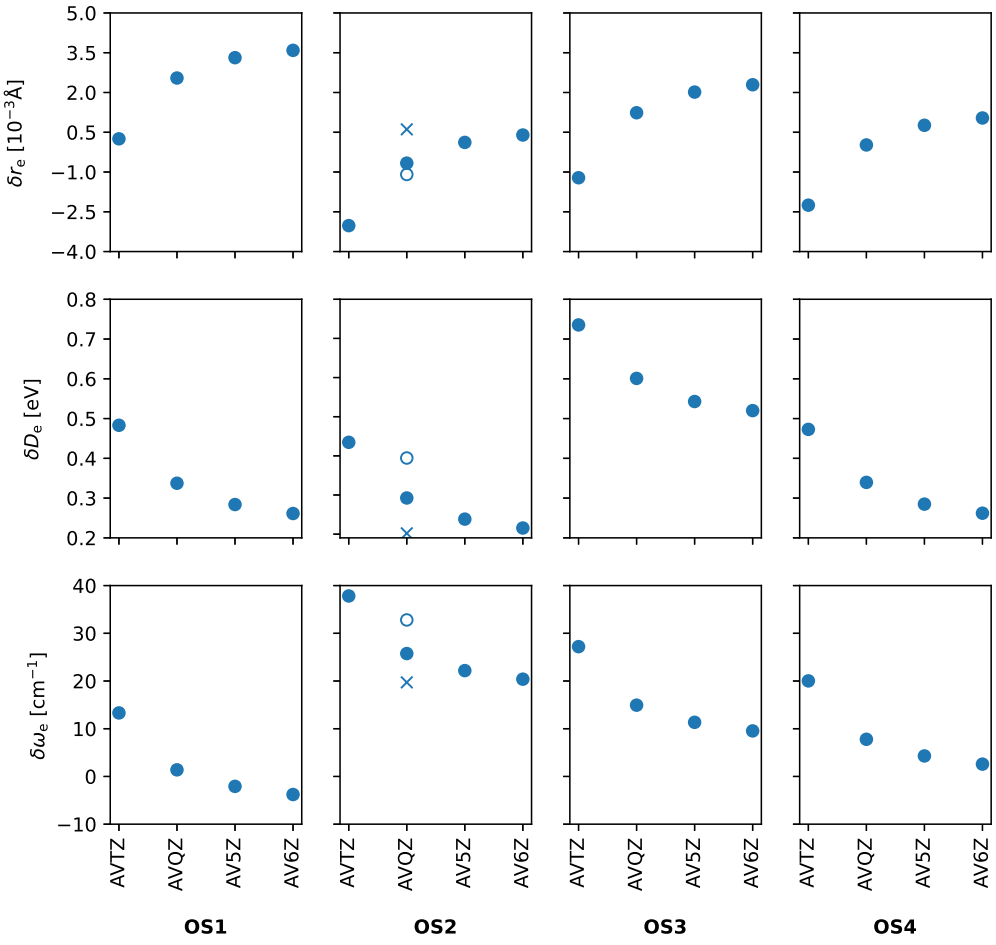

Figure 4: The same as in figure 1, but for the A $^2\Pi_u$ state of the N_2^+ ion.

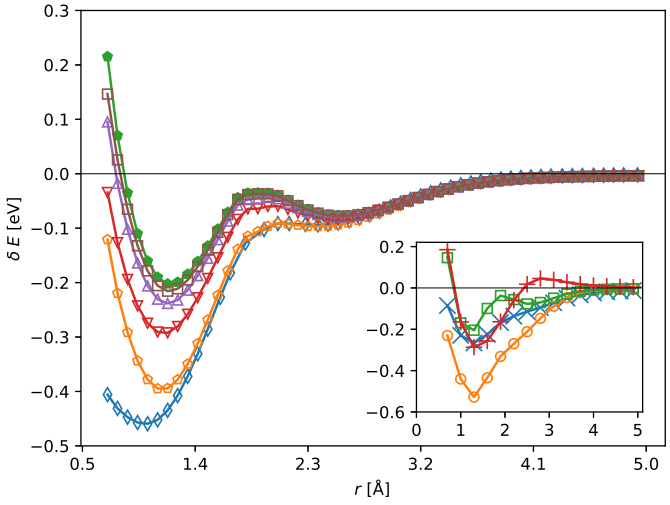

Figure 5: The same as in figure 2, but for the A $^2\Pi_u$ state of the N_2^+ ion.

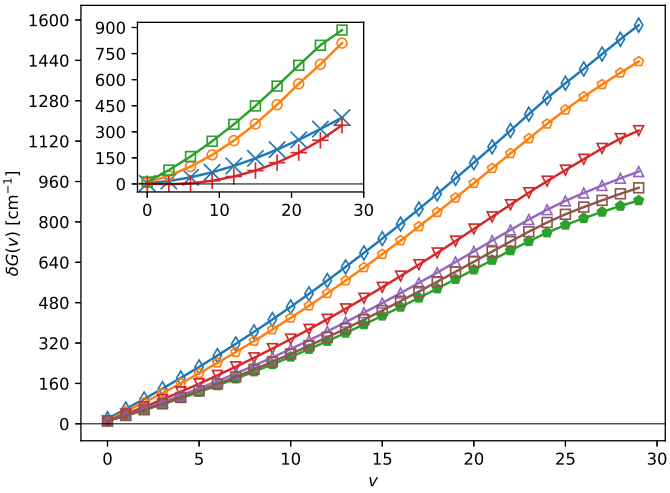

Figure 6: The same as in figure 3, but for the A $^2\Pi_u$ state of the N_2^+ ion.

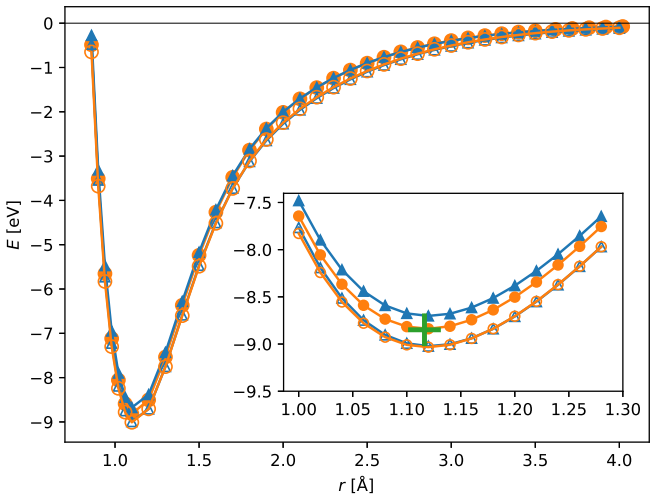

Figure 7: Comparison of MCSCF (empty symbols) and MRCI (full symbols) PECs calculated for the $X\,^2\Sigma_g^+$ state of the N_2^+ ion using AVQZ′/OS2 (blue triangles) and AV6Z/OS4 (orange circles). In the inset, a magnified view of the vicinity of the PEC minimum is depicted. The experimental value of the potential energy minimum (green plus) is taken from reference [19].

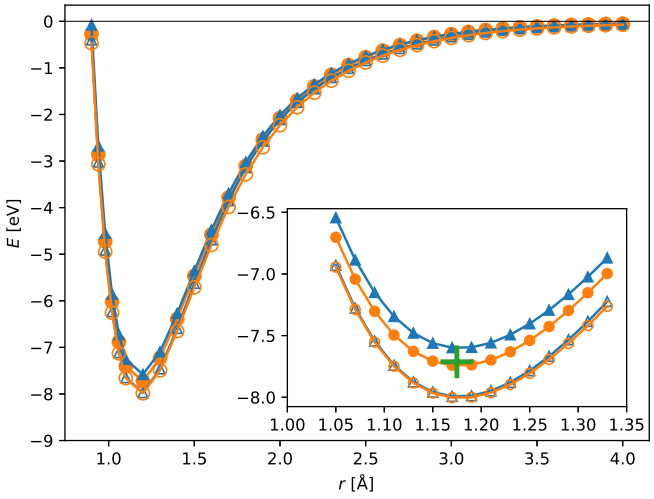

Figure 8: The same as in figure 7, but for the $A\,^2\Pi_u$ state of the N_2^+ ion.

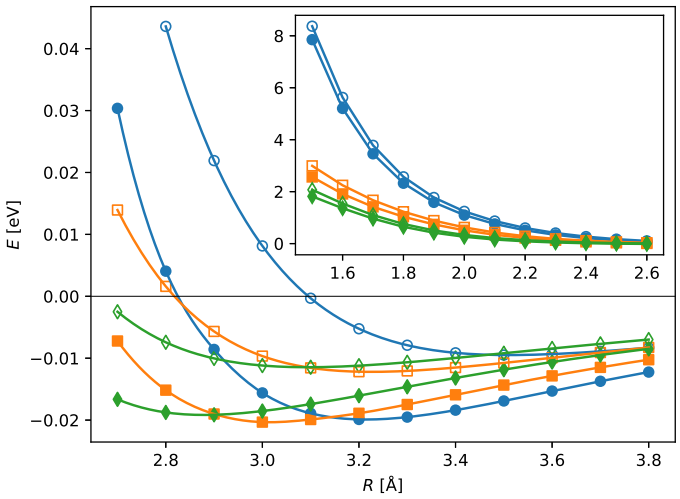

Figure 9: 1D cuts of the MCSCF (empty symbols) and MRCI (full symbols) PESs computed for the electronic ground state ($1A'$) of the N_2^+/He ion with the distance of nitrogen atoms fixed at $r = 1.1166$Å and for selected Jacobi angles, $\theta = 1°$ (blue circles), $\theta = 45°$ (orange squares), and $\theta = 90°$ (green diamonds). In the inset, the short-distance, repulsive walls of the calculated curves are depicted.

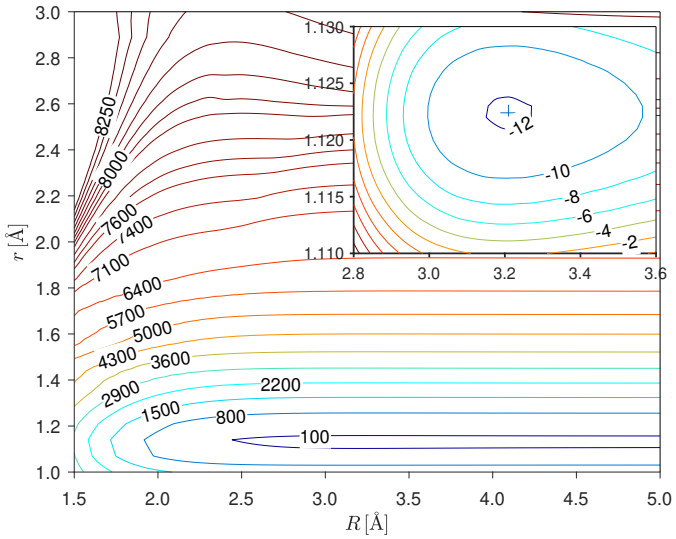

Figure 10: Contour plot of the N_2^+/He ground state PES ($1A'$) as obtained for the MCSCF/AVQZ′ method around its global minimum. Energies are given in meV and the asymptote corresponds to the N_2^+(equ) + He dissociated state (where "equ" indicates that the equilibrium distance of nitrogen atoms is considered as obtained at the same level of theory for the $N_2^+(X\,^2\Sigma_g^+)$ ion). A magnified view of the PES minimum is shown in the inset.

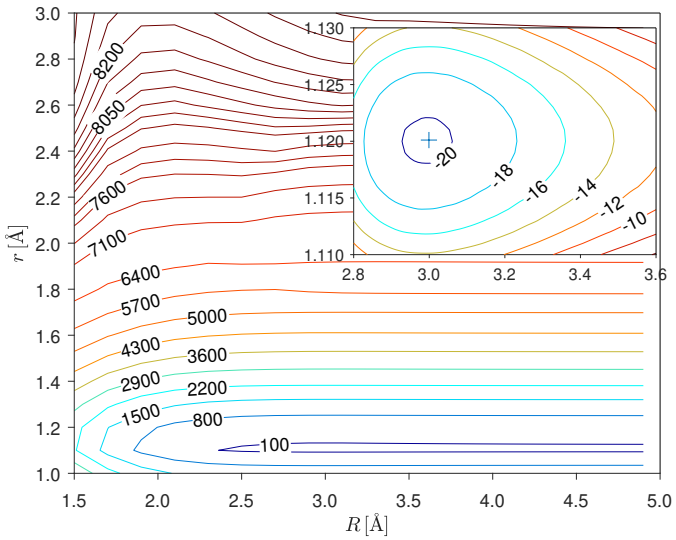

Figure 11: The same as in figure 10, but calculated at the MRCI/AVQZ′ level.

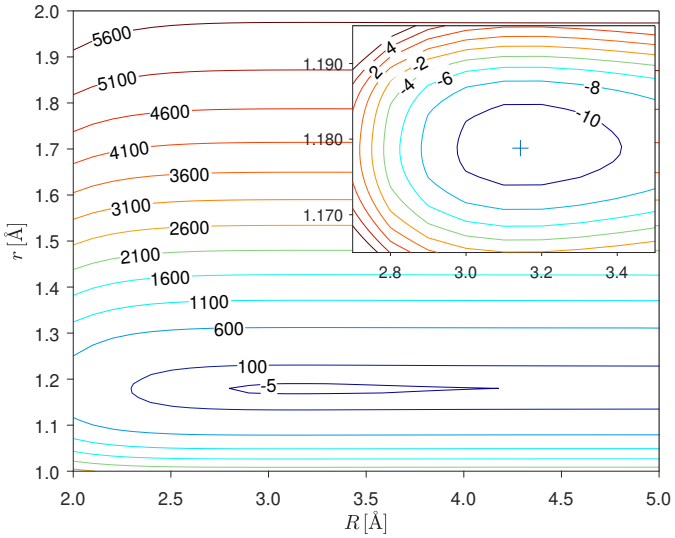

Figure 12: Contour plot of the N_2^+/He lowest PES of the $1A''$ symmetry as obtained for the MCSCF/AVQZ′ method. Like in figure 10, energies are given in meV and the asymptote corresponds to the N_2^+(equ) + He dissociated state.

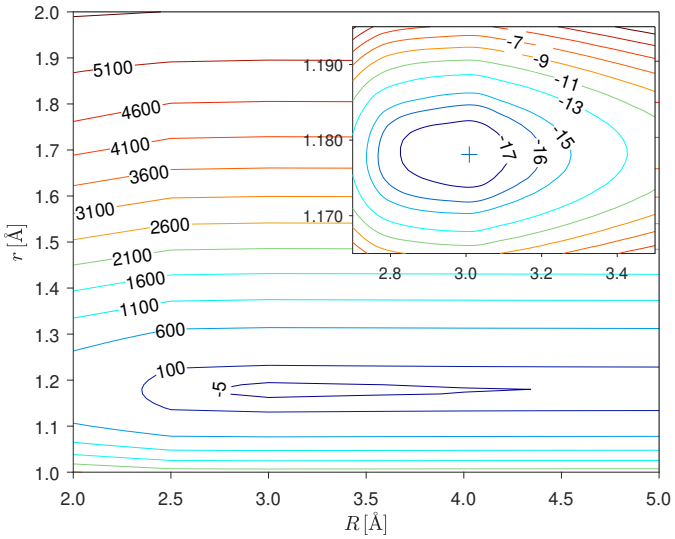

Figure 13: The same as in figure 12, but calculated at the MRCI/AVQZ′ level.

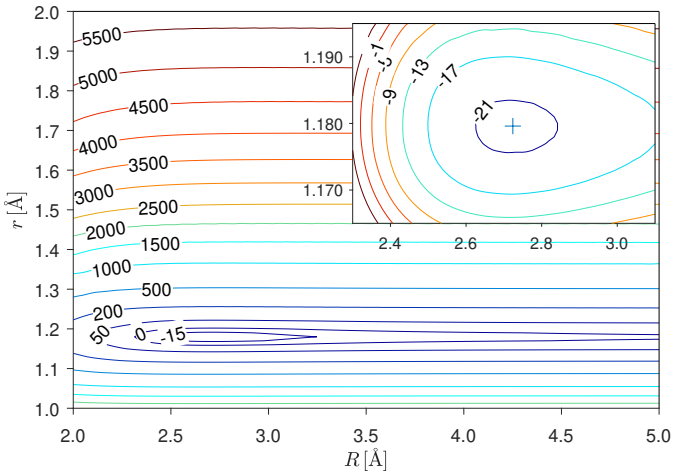

Figure 14: Contour plot of the lowest excited PES of the N_2^+/He ion in the A' symmetry ($2A'$) as obtained for the MCSCF/AVQZ′ method. Energies are given in meV, the asymptote corresponds to the N_2^+(equ) + He dissociated state.

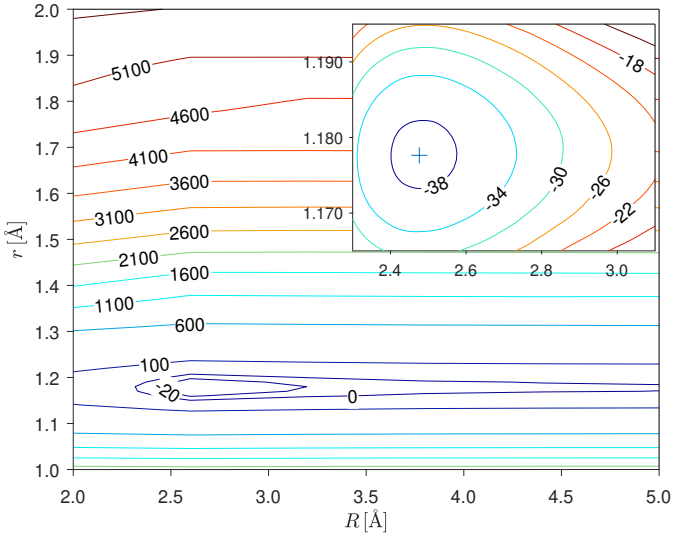

Figure 15: The same as in figure 14, but calculated at the MRCI/AVQZ′ level.